JOURNAL OF AIRCRAFT
Vol. 35, No. 2, March–April 1998

Reduced-Order Aerodynamic Model and Its Application to a Nonlinear Aeroelastic System

Deman Tang,* Mark D. Conner,† and Earl H. Dowell‡
Duke University, Durham, North Carolina 27708-0300

Starting from a finite state model for a two-dimensional aerodynamic flow over an airfoil, the eigenmodes of the aerodynamic flow are determined. Using a small number of these aerodynamic eigenmodes, i.e., a reduced-order model, the aeroelastic model is formed by coupling them to a typical section structural model with a trailing-edge flap. A free-play nonlinearity is modeled. Results are shown from the finite state model, the reduced-order model, and previous theoretical and experimental work. All results are in good agreement.

Nomenclature

b = semichord of the airfoil section, $c/2$
c = chord of the airfoil section
h, $\bar{h}$ = plunge displacement, h/b
L = lift force
M = size of reduced-order aerodynamic model
$M_{a,c/4}$ = torsional moment about the quarter-chord
M_r = reference mass/length of wing–aileron system
M_β = flap moment about the flap axis
N = number of inflow states
n = expansion index of the deformable airfoil
q = aerodynamic modal coordinate
t = time
U = airspeed
U_f = flutter airspeed
α = torsional angle of wing
β = flap rotational angle
δ = freeplay region
Λ = eigenvalue matrix
λ = induced flow velocity
λ_R, λ_I = real and imaginary part of the eigenvalue
λ^R, λ^L = right and left eigenvectors
ρ = air density
τ = nondimensional time, tU/b
ω_h, ω_α = plunge and torsional natural frequencies
ω_β = flap natural frequency
$\dot{}$ = d( )/dt
$'$ = d( )/dτ

Introduction

AN earlier theoretical/experimental study of an aeroelastic wing system with a trailing-edge flap including structural freeplay has been presented.[1] Following the work of Ref. 1, in the present paper we use Peters' finite state airloads model for a deformable airfoil[2] to replace the state-space model proposed by Edwards et al.[3] and previously used in Ref. 1. Peters' theory[2] allows for a thin airfoil performing small arbitrary motions with respect to a reference frame that can perform arbitrarily large translations and rotations in two dimensions. This aerodynamic model is derived from potential flow theory with no restrictive assumptions on the time history of airfoil motions. The aerodynamic states are the coefficients of a set of induced-flow expansions and are constructed as a set of first-order state equations that is easily coupled to the structural equations.

Although, as indicated in Ref. 4, excellent results for the unsteady aerodynamic forces were found with Peters' finite state model[2] with only a relatively few states when compared with those results obtained with Theodorsen and Wagner aerodynamic theories,[5] there is still an opportunity for improvement. Here, we explore how to retain the accuracy of Peters' aerodynamic model[2] while achieving a minimum number of states. The first important step was taken by Peters,[2] who used the least-squares method to obtain a set of first-order state equations from the potential flow theory. The second step is to extract the most important aerodynamic eigenmodes from the first-order state equations (following earlier work described in Ref. 6), that are then coupled with the structural equations.

This paper also considers the nonlinear aeroelastic phenomena of a typical airfoil section with control surface freeplay using this new aerodynamic model. The theoretical predictions indicate both a high-amplitude (low-frequency) and a low-amplitude (high-frequency) steady-state limit cycle oscillation. Between these two limit cycle oscillations there is an abrupt amplitude change, especially for the plunge motion, when the airspeed reaches a certain value. The low-frequency limit cycle suddenly becomes unstable, and the system is attracted to a stable, high-frequency limit cycle. The effect of the initial conditions on the nonlinear behavior is also discussed.

Peters developed a three-dimensional rotor wake model[7] that is also in finite state form.

State–Space Equations

A schematic of a typical airfoil section with a control surface at the trailing edge of the main wing is shown in Fig. 1. There is a structural freeplay nonlinearity that produces a piecewise linear change in the structural stiffness of the control surface as shown in Fig. 2. Because the aeroelastic typical section has three degrees of freedom (DOF), h, α, and β of the control surface, there are six structural DOFs in the state–space. The differential equations of motion in matrix form, Eq. (1), expressing the equilibrium of the moments about point a of the entire airfoil, of the moments on the control surface about point c, and of the vertical forces on the airfoil (Fig. 1), are as follows:

$$[M_s]\{\ddot{y}\} + [C_s]\{\dot{y}\} + [K_s]\{y\} + \{M_\beta\} = [S_1]\{F_a\} \quad (1)$$

Received Aug. 24, 1996; received June 15, 1997; accepted for publication Aug. 21, 1997.

*Research Associate, Department of Mechanical Engineering and Materials Science.
†Graduate Research Assistant, Department of Mechanical Engineering and Materials Science.
‡J. A. Jones Professor and Dean of the School of Engineering.

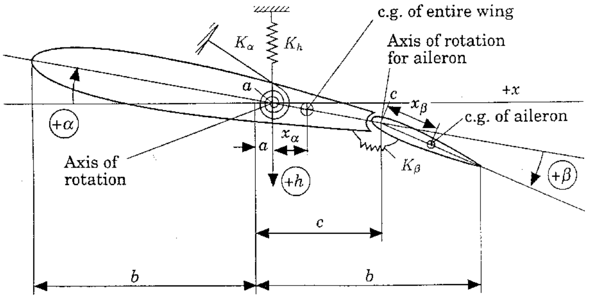

Fig. 1 Aeroelastic typical section with control surface.

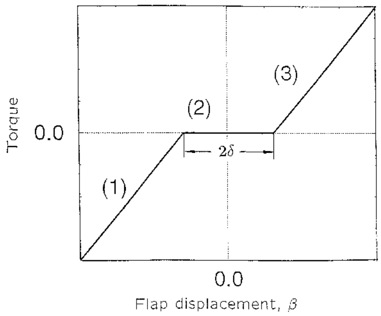

Fig. 2 Restoring moment caused by K_β with a symmetric freeplay region about $\beta = 0$.

where $\{y\}$ is expressed as $\{h, \alpha, \beta\}^T$, $\{M_\beta\} = \{0, 0, M_\beta\}^T$

$$[S_1] = \begin{bmatrix} 1/M_r b & 0 & 0 \\ 0 & 1/M_r b^2 & 0 \\ 0 & 0 & 1/M_r b^2 \end{bmatrix}$$

$$[K_s] = \begin{bmatrix} K_h & 0 & 0 \\ 0 & K_\alpha & 0 \\ 0 & 0 & \nu K_\beta \end{bmatrix}$$

When the structural freeplay gap δ is zero, then $\nu = 1$ and $M_\beta = 0$, and when the structural freeplay gap is not zero, then $\nu = 0$ and the control surface moment–rotation relationships may be expressed as

$$M_\beta = \begin{cases} K_\beta(\beta - \delta) & |\beta| \geq \delta, \quad \beta > 0 \\ K_\beta(\beta + \delta) & |\beta| \geq \delta, \quad \beta < 0 \\ 0 & \text{otherwise} \end{cases} \tag{2}$$

$[C_s]$ is the structural damping matrix. An attempt has been made here to include structural damping in the numerical model in a logical and physically meaningful way using viscous modal damping coefficients.[1]

The right-hand side (RHS) of Eq.(1) forms a vector of aerodynamic forces $\{\boldsymbol{F}_a\} = \{L, M_{\alpha,c/4}, M_\beta\}^T$. We use Peters' finite state incompressible airloads model for a deformable airfoil[2] to determine these aerodynamic forces. They are

$$\{\boldsymbol{F}_a\} = [T]^T\{L_m\} \tag{3}$$

where

$$\begin{aligned}\{L_m\} &= 2\pi\rho b U \lambda_a\{c_1\} - 2\pi\rho U^2[K][T]\{y\} \\ &\quad - 2\pi\rho b U[C][T]\{\dot{y}\} - \pi\rho b^2[M][T]\{\ddot{y}\} \\ &= \lambda_a\{p\} - [K_a]\{y\} - [C_a]\{\dot{y}\} - [M_a]\{\ddot{y}\}\end{aligned}$$

For matrices $[T]$, $\{c_1\}$, $[K]$, $[C]$, and $[M]$ (see Ref. 2). The induced flow velocity λ_a is approximately determined by

$$\lambda_a \approx \frac{1}{2}\sum_{i=1}^{N} b_i\lambda_i \tag{4}$$

The closed-form expressions for the b_i are given in Appendix C of Ref. 4. The result of Peters' analysis is a set of finite state equations for the aerodynamic unknowns in Peters' model (see Ref. 4), which are the in-flow velocity components, λ_i and λ_a

$$[A]\{\dot{\lambda}\} + (U/b)\{\lambda\} = [B_1]\{\ddot{y}\} + (U/b)[B_2]\{\dot{y}\} \tag{5}$$

where the matrix $[A]$ is given in Ref. 4, and

$$[B_1] = \{c_2\}\{s_2\}^T[T]$$

$$[B_2] = \{c_2\}\{s_3\}^T[T]$$

$$\{c_2\}_{N*1} = \{2, 1, 2/3 \,.\,.\,.\,.\,.\,.\,.\, 2/N\}^T$$

$$\{s_2\}^T_{1*n} = \{1, 1/2, 0, 0, 0 \,.\,.\,.\,.\, 0\}^T$$

$$\{s_3\}^T_{1*n} = \{0, 1, 2, 3 \,.\,.\,.\,.\,.\,.\, n - 1\}^T$$

Equation (5) is basically an equation for the time evolution of vortex transport in the wake of the airfoil. Combining Eqs. (1–5), and defining $X_e = \{\dot{y}, y, \lambda\}^T$, we obtain a set of state–space equations with six structural states and N inflow states. These equations are

$$\dot{X}_e = A_e X_e + B_e \tag{6}$$

where

$$A_e = \begin{bmatrix} M_e & C_e & 0 \\ 0 & M_e & 0 \\ -B_1 & -\dfrac{U}{b}B_2 & A \end{bmatrix}^{-1} \begin{bmatrix} 0 & -K_e & B_n \\ M_e & 0 & 0 \\ 0 & 0 & -\dfrac{U}{b}I \end{bmatrix}$$

$$B_e = \begin{bmatrix} M_e & C_e & 0 \\ 0 & M_e & 0 \\ -B_1 & -\dfrac{U}{b}B_2 & A \end{bmatrix}^{-1} \begin{Bmatrix} 0 \\ -M_\beta \\ 0 \end{Bmatrix}$$

where submatrices M_e, K_e, and C_e are the equivalent mass, stiffness, and damping matrices composed of structural and aerodynamic components, $M_e = [M_s] + [M_a]$, $C_e = [C_s] + [C_a]$, and $K_e = [K_s] + [K_a]$.

Reduced-Order Aerodynamic Model

Reduced-Order Technique

If we assume the structural response to be zero, then from Eq. (5) one obtains a representation of free fluid motion

$$[A]\{\dot{\lambda}\} + (U/b)\{\lambda\} = \{0\} \tag{7}$$

Defining a τ normalized on b, and the freestream velocity U, then $\tau = tU/b$ and

$$\dot{\lambda} = \frac{U}{b}\frac{d\lambda}{d\tau} = \frac{U}{b}\lambda'$$

Thus, Eq. (7) becomes

$$[A]\{\lambda'\} = -[I]\{\boldsymbol{\lambda}\} \tag{8}$$

From Eq. (8), an aerodynamic eigenvalue problem may be formed.

Because the matrix $[A]$ is nonsymmetric, we must compute the right and left eigenvalues and eigenvectors of the generalized eigenvalue problem. They are

$$[A][\lambda^R]\Lambda = -[I][\lambda^R] \tag{9}$$

$$[A]^T[\lambda^L]\Lambda = -[I][\lambda^L] \tag{10}$$

where $[\lambda^R]$ and $[\lambda^L]$ are the right and left eigenvector matrices, respectively, and Λ is a diagonal matrix whose diagonal entries contain the eigenvalues, and $[I]$ is a diagonal identity matrix.

The right and left eigenvectors are orthogonal with respect to the matrix $[A]$ and $[I]$. We normalize the eigenvectors such that they are orthonormal with respect to $[A]$. Therefore,

$$[\lambda^L]^T[A][\lambda^R] = [I] \tag{11}$$

$$[\lambda^L]^T[\lambda^R] = -[\Lambda] \tag{12}$$

Next, we let the induced flow vector $\{\boldsymbol{\lambda}\}$ be a linear combination of the m right eigenvectors (where in practice $m << N$), i.e.,

$$\{\boldsymbol{\lambda}\} = [\lambda_m^R]\{\boldsymbol{q}\} \tag{13}$$

where $\{\boldsymbol{q}\}$ is the vector of modal coordinates. Substitution of Eq. (13) into Eq. (5), premultiplying Eq. (5) by $[\lambda_m^L]^T$, and making use of the orthogonality conditions [Eqs. (11) and (12)], yields the new aeroelastic model

$$\begin{aligned} &[M_e]\{\ddot{y}\} + [C_e]\{\dot{\boldsymbol{y}}\} + [K_e]\{\boldsymbol{y}\} + \{M_\beta\} \\ &\quad - [B_m][\lambda_m^R]\{\boldsymbol{q}\} = \{0\} \\ &\{\dot{\boldsymbol{q}}\} + (U/b)[\Lambda]\{\boldsymbol{q}\} - [\lambda_m^L]^T([B_1]\{\ddot{\boldsymbol{y}}\} \\ &\quad + (U/b)[B_2]\{\dot{\boldsymbol{y}}\}) = \{0\} \end{aligned} \tag{14}$$

Let $X_d = \{\dot{\boldsymbol{y}}, \boldsymbol{y}, \boldsymbol{q}\}^T$. The resulting aeroelastic system of the reduced-order state variable equations is given by

$$\dot{X}_d = A_d X_d + B_d \tag{15}$$

where

$$A_d = \begin{bmatrix} M_e & C_e & 0 \\ 0 & M_e & 0 \\ -B_3 & -\dfrac{U}{b}B_4 & I \end{bmatrix}^{-1} \begin{bmatrix} 0 & -K_e & B_m \\ M_e & 0 & 0 \\ 0 & 0 & -\dfrac{U}{b}\Lambda \end{bmatrix}$$

$$B_e = \begin{bmatrix} M_e & C_e & 0 \\ 0 & M_e & 0 \\ -B_3 & -\dfrac{U}{b}B_4 & I \end{bmatrix}^{-1} \begin{Bmatrix} 0 \\ -M_\beta \\ 0 \end{Bmatrix}$$

where

$$B_3 = [\lambda^L]^T[B_1], \qquad B_4 = [\lambda^L]^T[B_2], \qquad B_m = [B_n][\lambda^R]$$

Static Correction Technique

One finds that with the reduced-order model, the first few aerodynamic eigenmodes (those having very small aerodynamic damping) must be retained in the model to obtain accurate results. However, while the dominant eigenmodes have been retained, all of the eigenmodes participate in the response to some degree. To account for the neglected eigenmodes, therefore, we use a quasistatic correction that may account for much of their influence. This technique is similar to the mode-acceleration method common to structural dynamics and was first suggested in the context of fluid eigenmode analysis by Hall and Florea.[8] Thus, let

$$\{\boldsymbol{\lambda}\} = \{\lambda_s\} + \{\lambda_d\} \tag{16}$$

The first term on the RHS is a quasistatic solution of the induced flow, and the second term is a dynamic perturbation solution. From Eq. (5), $\{\lambda_s\}$ is defined by

$$\{\lambda_s\} \equiv (b/U)([B_1]\{\ddot{y}\} + (U/b)[B_2]\{\dot{y}\}) \tag{17}$$

Substitution of Eqs. (16) and (17) into Eq. (5) gives an equation for λ_d

$$[A]\{\dot{\lambda}_d\} + (U/b)\{\lambda_d\} = -[A]\{\dot{\lambda}_s\} \tag{18}$$

Expanding λ_d in terms of the eigenmodes gives

$$\{\lambda_d\} = [\lambda_m^R]\{\boldsymbol{q}\} \tag{19}$$

and for $X_s = \{y, \dot{y}, \ddot{y}, q\}^T$, the resulting system of reduced-order aeroelastic equations with a static correction to the aerodynamic model is given by

$$G_s\dot{X}_s = A_sX_s + B_s \tag{20}$$

where

$$A_s = \begin{bmatrix} -K_e & 0 & 0 & -B_m \\ 0 & M_s & 0 & 0 \\ 0 & 0 & q_d & 0 \\ 0 & 0 & 0 & \dfrac{U}{b}\Lambda \end{bmatrix}$$

$$G_s = \begin{bmatrix} C_s & M_s & 0 & 0 \\ M_s & 0 & 0 & 0 \\ 0 & q_d & 0 & 0 \\ 0 & q_c & q_d & I \end{bmatrix}$$

$$B_s = \{-M_\beta, 0, 0, 0\}^T$$

$$M_s = [M_e] - (b/U)[B_n][B_1]$$

$$C_s = [C_e] - [B_n][B_2]$$

$$q_c = [\lambda^L]^T[A][B_2]$$

$$q_d = [\lambda^L]^T[A][B_1]$$

Numerical Results

The parameters of the numerical model comes from the experimental model previously described.[1] The nominal values for the inertial, stiffness, and damping parameters of the experimental structural system were measured. A summary of the system parameters is given in the following:

Geometry parameters:
- Chord = 0.254 m
- span = 0.52 m
- b = 0.127
- Elastic axis (a) with respect to (b) = −0.5
- Hinge line (c) with respect to (b) = 0.5

Mass parameters:
- Mass of wing = 0.62868 kg
- Mass of aileron = 0.18597 kg
- Mass/length of wing–aileron = 1.558 kg
- (Mass of support blocks) = (0.47485 × 2 kg)

Inertial parameters:
S_α (per span) = 0.08587 kg m
S_β (per span) = 0.00395 kg m
x_α = 0.434
x_β = 0.01996
I_α (per span) = 0.01347 kg m^2
I_β (per span) = 0.0003264 kg m^2
r_α = 0.7321
r_β = 0.11397
κ = 0.03984
Stiffness parameters:
K_α (per span) = 1486 1/s^2
K_β (per span) = 155 1/s^2
K_h (per span) = 1809 1/s^2
Damping parameters:
ζ_α (half-power) = 0.01626
ζ_β (half-power) = 0.0115
ζ_h (half-power) = 0.0113

A comparison of the structural natural frequencies for the numerical and experimental systems is given in Table 1.

Stability of the Linear Aeroelastic Model

When the freeplay gap is zero, a linear aeroelastic model is obtained. For the linear system as given by Eqs. (6), (15), and (20), the nonlinear terms B_e, B_d, and B_s are set to zero, and for the coefficient in the structural stiffness submatrix, $\nu = 1$. The eigenvalues of the A_e or A_d determine the stability of the system. When the real part of any one eigenvalue becomes positive, the entire system becomes unstable. Note that in Eq. (20), because G_s is noninvertible, we change Eq. (20) to

$$A_s^{-1}G_s\dot{X}_s = X_s \tag{21}$$

The inverted eigenvalues of the $A_s^{-1}G_s$ can also determine the stability of this system. For Eq. (21), numerical results are shown in Fig. 3. In Peters' induced flow model,[2] we use the augmented closed-form to calculate the coefficients b_i. The number of inflow states is taken as $N = 10$, and the expansion index, $n = 10$ (Ref. 2). The computation used double-precision arithmetic. In Fig. 3, the abscissa indicates the size of the reduced-order aerodynamic model M, and also N for Peters' model.[2] The ordinate indicates the ratio of the flutter velocity to the flutter velocity obtained from Peter's model for $N = 10$,

Table 1 Coupled natural frequencies

	Numerical, Hz	Experimental, Hz	% Difference
ω_α(coupled)	9.218	9.125	1.02
ω_β(coupled)	19.442	18.625	4.39
ω_h(coupled)	4.455	4.375	1.82

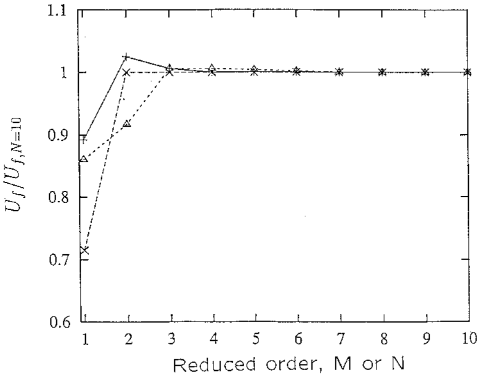

Fig. 3 Relative flutter speed to the flutter speed obtained from Peters' model[2] of N = 10 vs M, or N. +, reduced-order model; ×, reduced-order model with static correction; and Δ, Peters' model.

which is equal to U_f = 23.81 m/s (Ref. 2). It is interesting to note that when $M = 2$ and the static correction is included, the present results are in excellent agreement with the result for Peters' model when $N = 10$ (Ref. 2). However when $N = 2$ for Peters' model,[2] the corresponding ratio is 0.915 (Fig. 3). Thus, the present model has greater accuracy for a smaller number of aerodynamic states.

Figure 4 shows a typical graphical representation of the eigenanalysis in the forms of λ_R vs the velocity and also a root–locus plot for the nominal linear system using a reduced-order model with $M = 4$. The solutions are assumed in the form of $e^{\lambda t}$. There is an intersection of λ_R with the velocity axis, U_f = 23.81 m/s, which is the flutter critical velocity with the corresponding flutter oscillatory frequency ω_f = 38.5 rad/s (6.13 Hz). By contrast, the experimental flutter speed and frequency are 20.57 m/s and 5.47 Hz, respectively. The numerical results are approximately 15 and 12% higher than the experimental values. The most likely sources for these differences are physical phenomena, including inherent structural nonlinearities, that are not incorporated into the present theoretical model. These nonlinearities are evidenced by the fact that at speeds near the flutter boundary, a small perturbation of the linear system may result in decaying oscillations, while a slightly larger perturbation could lead to divergent motion. Other reasons for theoretical/experimental differences may be a low estimate of the structural damping as a result of neglecting the dry friction in the rotational link mechanism (bearings), and also to neglecting possible three-dimensional aerodynamic wall effects.

There are seven curves for the real parts of the eigenvalues denoted by a, b, c and d_1, d_2, d_3, d_4, as marked in Fig. 4. To determine the modal content of these results, the corresponding eigenvectors were examined. It was determined that curve a is dominated by the plunge motion of this model, b by the torsion, c by the flap rotation, and d_1, d_2, d_3, d_4 by aerodynamic

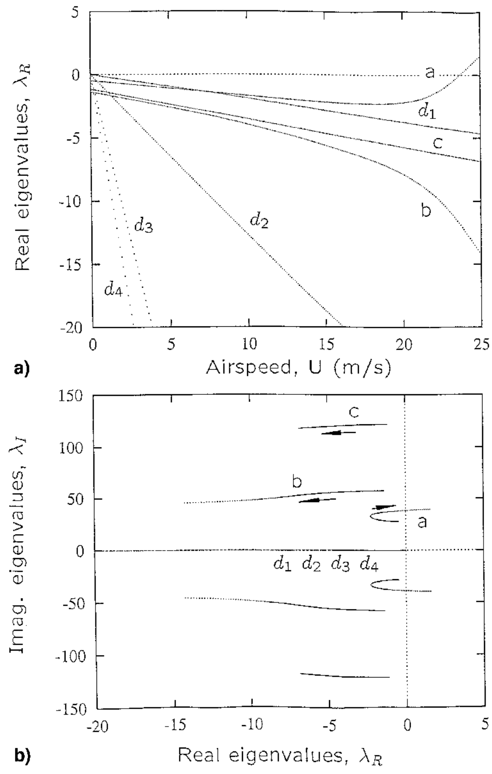

Fig. 4 Eigenvalue solutions of the linear system for using reduced-order model with M = 4. a) Real part and b) root–locus; line a is dominated by the plunge, line b by the torsion, line c by the flap rotation, and lines d_1, d_2, d_3, and d_4 by the induced-flow aerodynamics. The arrows indicate the direction of motion of the loci when U increases.

inflow modal behavior per se. From Fig. 4, it is found that the linear flutter is dominated by the plunge motion, although other zero airspeed or in vacuo modes are also present to some degree. Figure 4b is the locus of roots for this case.

Nonlinear Model

We used a standard Runge–Kutta algorithm in conjunction with the Peters' aerodynamic model,[2] Eq. (6), and the present reduced order model, Eq. (15), for time integrating the nonlinear equations. To determine the nonlinear behavior of the typical airfoil section with control surface freeplay, a comparison has been made using different aerodynamic models and different reduced-order numbers. A typical example for $U = 0.49 \times U_f$ and a freeplay region of $\delta = \pm 2.12$ deg is shown in Fig. 5. Figures 5a–5c are steady-state limit cycle oscillations under the same nonzero initial conditions in flap, which served to excite the system. The results are very close for the reduced-order model of $M = 2$ and 4, and the Peters' model[2] of $N = 10$. The most significant, but still small, difference comes from the initial phase shift and static equilibrium position of the system that is caused primarily by the quasistatic aerodynamic forces used in the reduced-order aerodynamic model.

Comparisons with the experimental results have been made for varying degrees of control surface freeplay. Three freeplay configurations were studied theoretically and experimentally, corresponding to freeplay regions of ± 1.15, ± 1.83, and ± 2.12 deg (Gap 1, Gap 2, and Gap 3, respectively). For each of the three cases, the model was placed in the wind tunnel such that the control surface was resting at one edge of the freeplay region. As the airflow in the tunnel was increased, this nonzero initial condition in the flap served to excite the system, causing the wing to settle into a steady-state limit cycle. The airflow was slowly increased to a new value and reached a new steady-

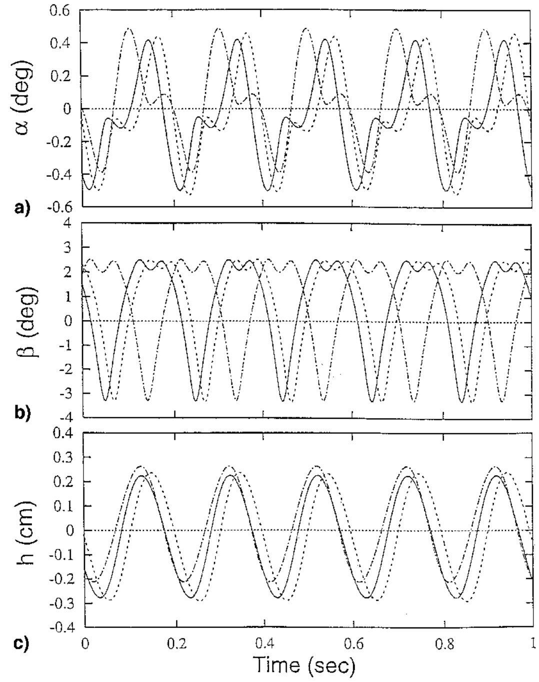

Fig. 5 Limit cycle oscillations for $U = 0.49 \times U_f$ and $\delta = \pm 2.12$ deg: a) torsion, b) flap rotation, and c) plunge. --, $M = 2$; —, $M = 4$ of reduced-order model; and -·-, Peters' model[2] with $N = 10$.

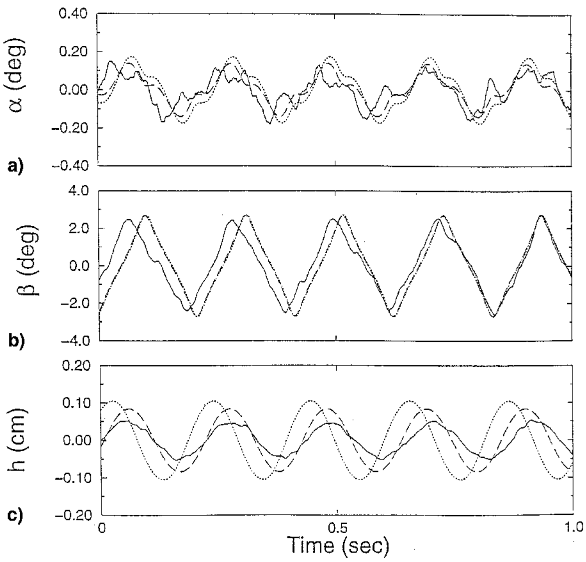

Fig. 6 Limit cycle oscillations for $U = 0.27 \times U_f$ and $\delta = \pm 2.12$ deg: a) torsion, b) flap rotation, and c) plunge. --, reduced-order model with $M = 4$, ···, Ref. 1; and ——, experiment.

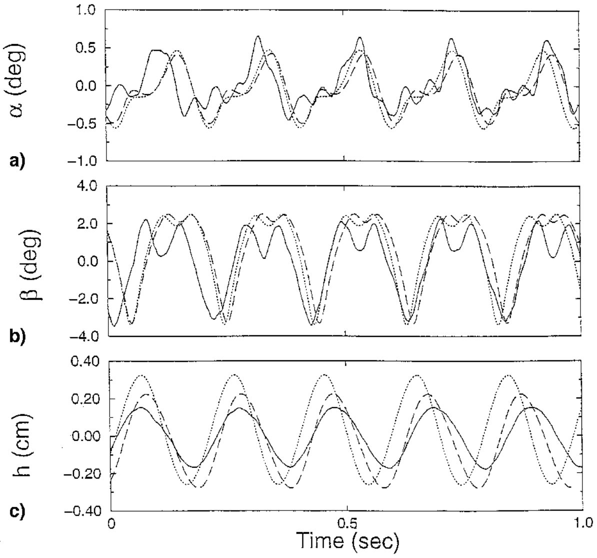

Fig. 7 Limit cycle oscillations for $U = 0.49 \times U_f$ and $\delta = \pm 2.12$ deg: a) torsion, b) flap rotation, and c) plunge. --, reduced-order model with $M = 4$; ···, Ref. 1; and ——, experiment.

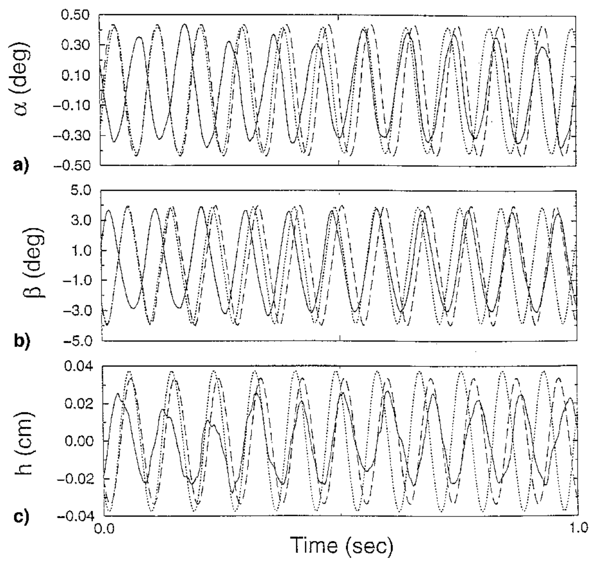

Fig. 8 Limit cycle oscillations for $U = 0.73 \times U_f$ and $\delta = \pm 2.12$ deg: a) torsion, b) flap rotation, and c) plunge. --, reduced-order model with $M = 4$; ···, Ref. 1; and ——, experiment.

state limit. The behavior of the system was examined at a variety of freesteam conditions below the linear flutter speed.

Four different types of motion were found from both the numerical predictions and experiments. For low velocities, $U < 0.18 \times U_f$ (theory) or $U < 0.23 \times U_f$ (experiment), giving the model an initial disturbance resulted in decaying oscillations that damped out to zero fairly quickly.

At $U \approx 0.18 \times U_f$ (theory) or $U \approx 0.23 \times U_f$ (experiment), there is a discrete jump from damped motion to a low-frequency limit cycle that is characterized by period one oscillations in the control surface degree of freedom. Figure 6 shows an example of experimental and numerical time series (the present method and the Ref. 1 method) for this limit cycle behavior for $U = 0.27 \times U_f$. The two numerical results are close to each other and there is slightdifference in the oscillation frequencies between the theory and experiment, but the numerical results do fairly accurately predict both the qualitative and quantitative behavior found experimentally. As the airflow increases further, the limit cycle amplitude in all three DOFs increases. This behavior is observed until the airflow speed reaches approximately $0.53 \times U_f$. Characteristic experimental and numerical time series for this motion are given in Fig. 7 for $U = 0.49 \times U_f$. A wide variety of initial disturbances was applied to the theoretical and experimental systems and, in each case, the systems settled into the same limit cycle behavior.

At $U \approx 0.55 \times U_f$, both for the theoretical and experimental systems, there is another abrupt change in the system behavior. The low-frequency limit cycle suddenly becomes unstable, and the system is attracted to a stable, high-frequency limit cycle. There is a dramatic drop in the plunge amplitude at this point. Near this point, the torsion amplitude has a small but complex change, while the flap amplitude jumps to a higher level and remains fairly constant.

For velocities between $U \approx 0.56 \times U_f$ and $U \approx 0.93 \times U_f$, a high-frequency limit cycle oscillation was observed. Again, a number of initial conditions were applied, each resulting in the same limit cycle behavior. In this velocity region, typical experimental and numerical time histories are shown in Fig. 8. Numerical simulations for this set of system parameters indicate that the nonlinear divergent flutter speed is within 2% of the linear boundary.

Summarizing the preceding four different types of motion, a limit cycle amplitude vs airflow speed ratio is shown in Fig. 9. Figure 9a–9c shows the torsional motion of the wing, the flap rotation, and the plunge motion, respectively. The amplitudes shown are based on rms calculations over one cycle of the numerical and experimental steady-state time histories. The results obtained from Ref. 1 are also plotted in Fig. 9 for comparison of the effects of the two different aerodynamic models on the nonlinear behavior of the same aeroelastic/structural system. The numerical results both from Ref. 1 and the present method are in reasonably good agreement with the experiment.

Figure 10 shows that the limit cycle frequencies for all of the experimental freeplay regions and the numerical models are very consistent. The onset of several limit cycles in the experimental model occur at freestream velocities that are near the onset of the same limit cycles in the numerical model for the present method and approximately 10% higher than those of Ref. 1.

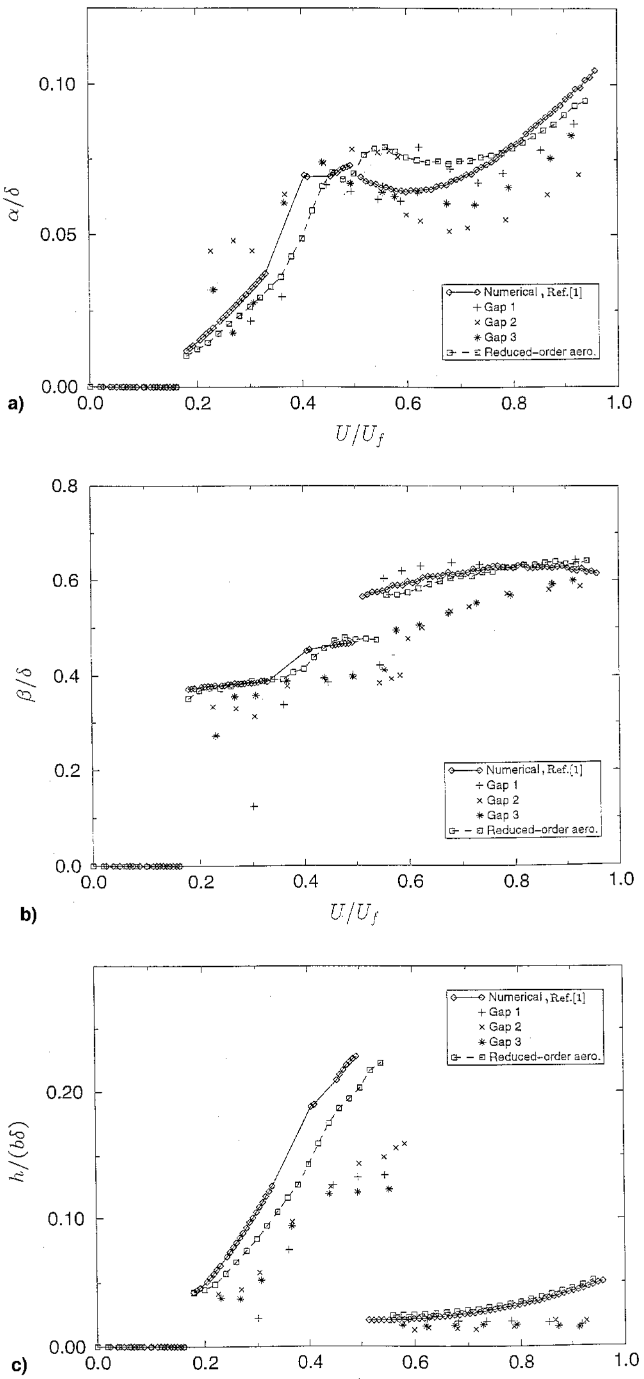

Fig. 9 Limit cycle amplitudes vs relative airspeed U/U_f: a) torsion, b) flap rotation, and c) plunge. + (Gap 1), × (Gap 2), and * (Gap 3) are from experiment; ◇ are from Ref. 1 and □ are from reduced-order model with $M = 4$.

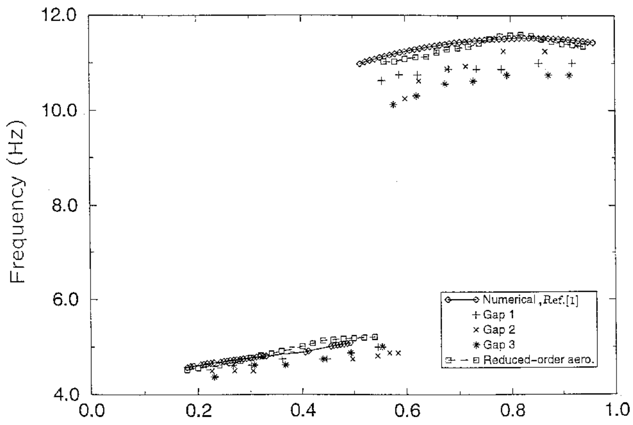

Fig. 10 Limit cycle frequency vs relative airspeed U/U_f: a) torsion, b) flap rotation, and c) plunge. + (Gap 1), × (Gap 2), and * (Gap 3) are from experiment; ◇ are from Ref. 1, and □ are from reduced-order model with $M = 4$.

Concluding Remarks

The finite state airload model for a deformable airfoil has been successfully applied to the case of a three DOF typical section including trailing-edge flap freeplay. A numerical model for predicting linear and nonlinear flutter behavior and limit cycle oscillations has been constructed and verified experimentally. The results fairly accurately predict the qualitative and quantitative behavior found experimentally.

As a novel feature of the present work, a reduced-order aerodynamic technique has been adapted to the state–space theory for the airloads. The results improved the computational accuracy while using a number of minimum aerodynamic states that are then incorporated into the nonlinear aeroelastic model. The present method for representing the aerodynamic forces is particularly attractive for development of a variety of control algorithms and flutter suppression for a fixed wing, and also can be extended to a three-dimensional induced flow model for the development of more accurate and computationally efficient predictions of rotor blade stability and forced response in helicopter aeroelastic problems.

Acknowledgments

This work was supported under the U.S. Air Force Office of Scientific Research Grant F49620-97-1-0063, Limit Cycle Oscillations and Nonlinear Aeroelastic Wing Response, and NASA Langley Grant, NAG 1 1569, Flutter of Wing and Control Surface with Freeplay. C. I. Jim Chang and Brian Sanders and Donald Keller are the respective Grant Monitors. The authors would also like to thank David Peters for his very helpful discussion of his work that has been the basis for our extension of his approach.

References

[1]Conner, M. D., Tang, D. M., Dowell, E. H., and Virgin, L. N., "Nonlinear Behavior of a Typical Airfoil Section with Control Surface Freeplay: A Numerical and Experimental Study," *Journal of Fluids and Structures*, Vol. 11, 1997, p. 89–109.

[2]Peters, D. A. "Finite-State Airloads for Deformable Airfoils on Fixed and Rotating Wings," Symposium on Aeroelasticity and Fluid/Structure Interaction, ASME Winter Annual Meeting, Chicago, IL, Nov. 1994.

[3]Edwards, J. W., Ashley, H., and Breakwell, J. V., "Unsteady Aerodynamic Modeling for Arbitrary Motions," *AIAA Journal*, Vol. 17, No. 4, 1979, pp. 365–374.

[4]Peters, D. A., and Cao, W. M., "Finite State Induced Flow Models, Part I: Two-Dimensional Thin Airfoil," *Journal of Aircraft*, Vol. 32, No. 2, 1995, pp. 313–322.

[5]Theodorsen, T., and Garrick, I. E., "Flutter Calculations in Three Degree of Freedom," NACA Rept. 741, June 1941.

[6]Dowell, E. H., "Eigenmode Analysis in Unsteady Aerodynamics: Reduced Order Models," *AIAA Journal*, Vol. 34, No. 8, 1996, pp. 1578–1588.

[7]Peters, D. A., and He, C. J., "Finite State Induced Flow Models, Part II: Three-Dimensional Rotor Disk," *Journal of Aircraft*, Vol. 32, No. 2, 1995, pp. 323–333.

[8]Hall, K. C., and Florea, R., "Reduced Order Modeling of Unsteady Flows About Airfoils," Symposium on Aeroelasticity and Fluid/Structure Interaction ASME Winter Annual Meeting, Chicago, IL, Nov. 1994.